Int. J. Electrochem. Sci., 15 **(2020)** 1338 – 1346, doi: 10.20964/2020.02.32

International Journal of
ELECTROCHEMICAL
SCIENCE
www.electrochemsci.org

Performance and Transport Characteristics of Solid Oxide Fuel Cells with Counter Flow Arrangement

Shian Li[1], *Rongqiang Wei*[1], *Hao Wang*[1], *Yuanxin Qi*[2], *Guogang Yang*[1,*], *Qiuwan Shen*[1,*]

[1] Marine Engineering College, Dalian Maritime University, Dalian, China;
[2] Department of Energy Sciences, Lund University, Lund, Sweden;
[*]E-mail:yanggg@dlmu.edu.cn and shenqiuwan@dlmu.edu.cn

Received: 6 October 2019 / *Accepted:* 26 November 2019 / *Published:* 31 December 2019

In this study, a two-dimensional model including the governing equations of mass, momentum, species, energy and charge, is developed and then applied to investigate the performance and multiphysics transport processes of solid oxide fuel cells with counter-flow arrangement. The current density and power density are calculated and presented, and the distributions of species and temperature are also analyzed. In addition, temperature distributions of fuel cells with varying operating temperature, anode inlet flow velocity and cathode inlet flow velocity are demonstrated. The results show that the temperature gradient increases with increasing operating temperature. And the local temperature decreases with increasing inlet flow velocities, especially the increasing cathode inlet flow velocity.

Keywords: Solid oxide fuel cells, Transport phenomena, Counter flow, Temperature gradient

1. INTRODUCTION

Solid oxide fuel cells (SOFCs) and proton exchange membrane fuel cells (PEMFCs) are typical high temperature and low temperature fuel cells, respectively [1-3]. Only hydrogen can be used as the fuel for PEMFCs, while a broad variety of fuel can be used in SOFCs via reforming reactions.

The cell performance of SOFCs can be easily obtained and evaluated by using experimental measurements. However, the transport phenomena inside fuel cells are not easy to be obtained due to the compact structure and small dimension. Numerical simulations can be used to investigate the transport characteristics inside fuel cells. Experimental measurements were carried out to examine the performance of SOFCs under varying operating conditions [4]. The performance and transport characteristics of SOFCs at various operating conditions were systematically studied by using a mathematical model [5]. Effects of geometric parameters on overall performance and local transport characteristics were investigated by different researchers [6-8]. Numerous efforts were made to

improve the performance. Graded electrodes were used to enhance the cell performance of SOFCs [9-12]. The performance can be significantly improved by designing proper flow field. Therefore, different flow fields were designed and then systematically studied [13-16].

A high temperature gradient can lead to thermal stress which affects the performance of SOFCs. Accordingly, the deterioration of performance and lifetime may occur. A mathematical model was developed to study the species and temperature distributions inside SOFCs [17]. It was reported that the heat and mass transport phenomena of fuel cells can be significantly affected by the fuel utilization [18]. Although various experimental and numerical studies on SOFCs can be found in the open literature, the understanding of transport phenomena inside SOFCs is still needed. In this paper, a two-dimensional model is used to study the cell performance and transport phenomena inside anode-supported planar SOFCs with counter flow arrangement. In addition, temperature distributions of fuel cells with varying operating temperature, anode inlet flow velocity and cathode inlet flow velocity are systematically investigated.

2. MODEL DESCRIPTION

2.1 Physical model and assumptions

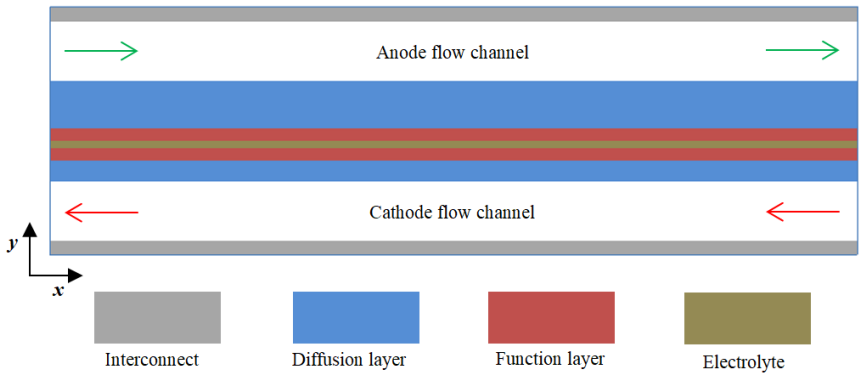

Figure 1. Schematic of a solid oxide fuel cell with counter-flow arrangement.

Table 1. Geometric parameters and the corresponding operating conditions

Parameters	Values / Unit
Length	40 mm
Interconnect thickness	0.3 mm
Channel thickness	1 mm
Anode/ Cathode DL thickness	0.38/0.05 mm
Anode/Cathode FL thickness	0.02/0.02 mm
Electrolyte thickness	0.01 mm
Operating pressure	1.0 atm
Operating temperature	1073 K

The computational domain used in this study is shown in Figure 1. And the geometric parameters and operating conditions are presented in Table 1. DL represents the diffusion layer and FL represents the function layer. The assumptions used in the mathematical model can be found in our previous study [5].

2.2 Governing equations

The governing equations and corresponding source terms are presented in Table 2 and Table 3. And the detailed descriptions of this model can be found in our previous study [5].

Table 2. The governing equations

Mass conservation equation:	$\nabla \cdot (\rho \vec{u}) = S_{mass}$
Momentum conservation equation:	$\nabla \cdot (\rho \vec{u}\vec{u}) = \nabla \cdot (\mu \nabla \vec{u}) - \nabla P + S_{mom}$
Species conservation equation:	$\nabla \cdot (\rho \vec{u} Y_i) = \nabla \cdot \left(\rho D_{eff,i} \nabla Y_i\right) + S_i$
Energy conservation equation	$\nabla \cdot \left(\rho c_p \vec{u} T\right) = \nabla \cdot \left(k_{eff} \nabla \mathrm{T}\right) + S_T$
Charge conservation equation:	$\nabla \cdot \left(\sigma_{eff,e} \nabla \phi_e\right) + S_e = 0$ $\nabla \cdot \left(\sigma_{eff,i} \nabla \phi_i\right) + S_i = 0$

Table 3. The sources terms of governing equations

$S_{mass} = S_{H_2} + S_{H_2O}$ (Anode) $S_{mass} = S_{O_2}$(Cathode)
$S_{mom} = -\frac{\mu}{K}\vec{u}$
$S_{H_2} = -\frac{j_a}{2F} M_{H_2}$ $S_{O_2} = -\frac{j_c}{4F} M_{O_2}$ $S_{H_2O} = \frac{j_a}{2F} M_{H_2O}$
$S_T = j_{a,c}\lvert\eta_{a,c}\rvert + j_{a,c}\frac{T\Delta S}{nF} + \sigma_{eff,i}\lVert\nabla\phi_i\rVert^2 + \sigma_{eff,s}\lVert\nabla\phi_s\rVert^2$
$S_e = -j_a$ $S_i = +j_a$ (Anode)
$S_e = +j_c$ $S_i = -j_c$ (Cathode)

2.3 Numerical implementation and boundary conditions

The commercial software ANSYS FLUENT is used for the implementation of fuel cell model. And the user defined functions (UDFs) are applied to describe the transport equations, source terms and the expressions in the mathematical model.

At the anode and cathode gas flow channel inlet, the velocity, temperature, and mass fractions are defined. At the anode and cathode gas flow channel outlet, a pressure-outlet boundary condition is prescribed. The electric potential, ϕ_e=0, is specified at the top wall, while the electric potential, ϕ_e=V_{cell}, is specified at the bottom wall. And the surrounding walls are adiabatic boundary condition. The corresponding boundary conditions are summarized and presented in Table 4.

Table 4. Boundary conditions

Description	Conditions	Value	Units
Anode terminal	Electrical	0	V
Cathode terminal	potential	0.7	V
Anode flow channel inlet	Velocity	0.3	m/s
	Mass fraction	H_2:H_2O=0.95:0.05	-
	Temperature	1073	K
Cathode flow channel inlet	Velocity	3	m/s
	Mass fraction	O_2:N_2=0.233:0.767	-
	Temperature	1073	K
Anode flow channel outlet	Pressure	0	Pa
Cathode flow channel outlet	Pressure	0	Pa

3. RESULTS AND DISCUSSION

For the model validation, the present model was carefully validated by comparing with the experimental study reported by Zhang et al. [19]. The results produced by the mathematical model shows good agreement with the data by the experiments. The detailed information of the model validation can be found in our previous study [5]. Therefore, the present mathematical model was applied in the following numerical simulations.

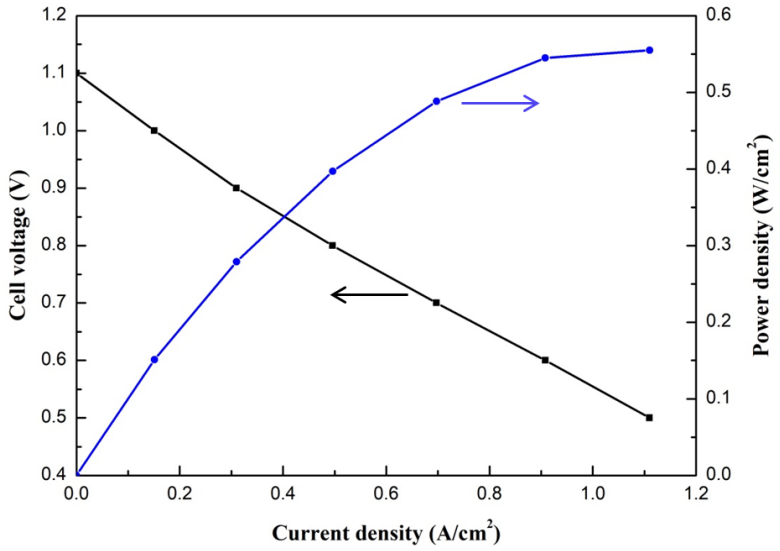

Figure 2. Performance of a SOFC with counter-flow arrangement.

The polarization curve is used to assess the cell performance. The performance of SOFCs with counter-flow arrangement is calculated and presented in Figure 2. It is clear seen that the current density increases with decreasing cell voltage and the power density increases with increasing current density. Due to the high operating temperature, the activation loss is very small. The trend of

polarization curve is mainly determined by the ohmic loss. The polarization curve of PEMFCs is quite different from that of SOFCs. The activation loss is dominated at low current densities [20-21]. The current density is 0.697 A/cm^2 at the cell voltage 0.7 V and the corresponding power density is 0.488 W/cm^2. The current density is 1.110 A/cm^2 at the cell voltage 0.5 V and the corresponding power density is 0.555 W/cm^2.

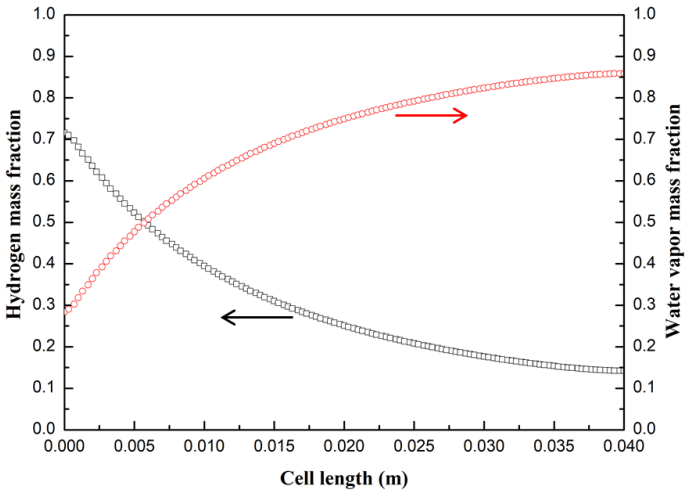

Figure 3. Hydrogen and water vapor mass fraction distributions of a SOFC with counter-flow arrangement at the cell voltage 0.7V.

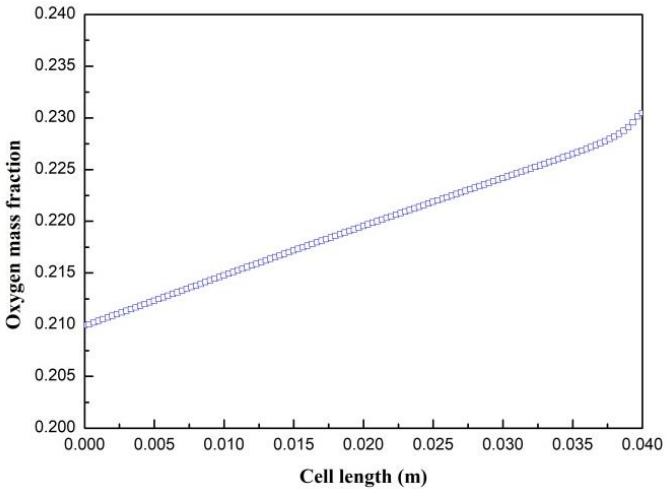

Figure 4. Oxygen mass fraction distribution of a SOFC with counter-flow arrangement at the cell voltage 0.7V.

The mass fraction distributions of hydrogen and water vapor along the x-coordinate direction at the cell voltage 0.7 V are given in Figure 3. It is clear that the hydrogen mass fraction gradually decreases and the water vapor mass fraction increases along the x-coordinate direction. This can be explained by the consumption of hydrogen and generation of water vapor due to the electrochemical reactions inside SOFCs. The hydrogen mass fraction decreases from 0.71 to 0.14, while the water vapor mass fraction increases from 0.29 to 0.86. Meanwhile, the mass fraction distribution of oxygen along the cathode side flow direction (from right to left) at the cell voltage 0.7 V is shown in Figure 4.

It can be seen that the oxygen mass fraction decreases along the flow direction due to the consumption caused by the electrochemical reactions. And the oxygen mass fraction decreases from 0.23 to 0.21. For both the co-flow and counter-flow arrangements of SOFCs, the mass fractions of hydrogen and oxygen decreases and the mass fraction of water vapor increases along the flow channel direction due to the electrochemical reactions [5, 22]. As shown in Figure 5, the local current density distribution along the x-coordinate direction is illustrated. It is clear that the local current increases firstly and then gradually decreases until the end of cell. This is attributed to the electrochemical reactions and flow arrangement. Similar distribution of local current density was also reported by Zhang et al. [22].

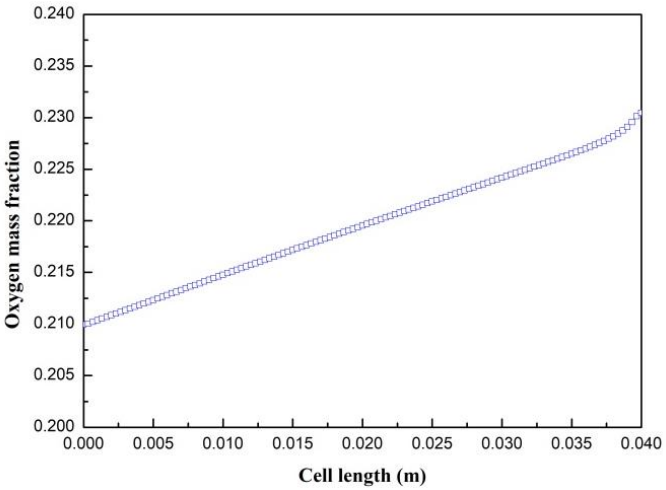

Figure 4. Oxygen mass fraction distribution of a SOFC with counter-flow arrangement at the cell voltage 0.7V.

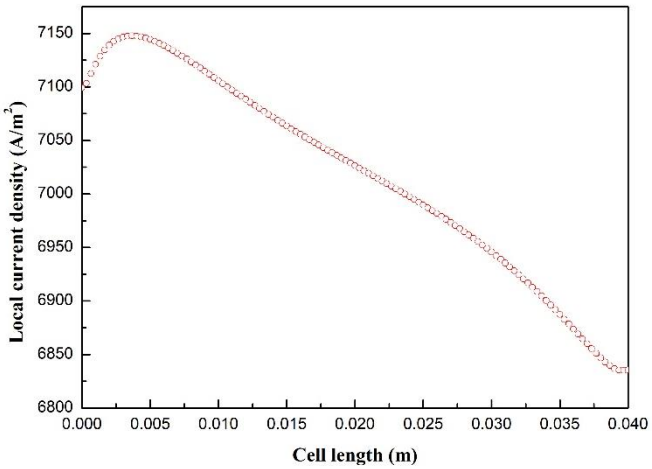

Figure 5. Local current density distribution of a SOFC with counter-flow arrangement at the cell voltage 0.7V.

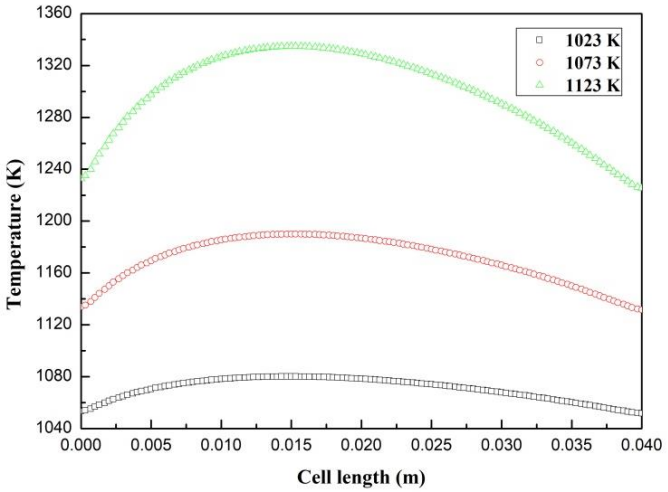

Figure 6. Temperature distributions at the anode DL and FL interface of SOFCs with different operating temperatures at the cell voltage 0.7V.

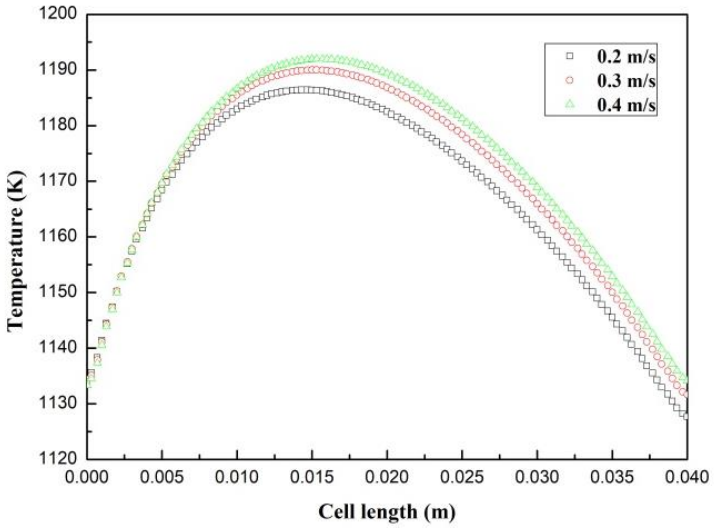

Figure 7. Temperature distributions at the anode DL and FL interface of SOFCs with different anode inlet flow velocities at the cell voltage 0.7V.

The local temperature distributions of SOFCs with co-flow arrangement under different operating temperature and anode/cathode velocity were systematically studied and reported in our previous study [5]. This paper focus on the effects of these factors on the temperature distributions of SOFCs with counter-flow arrangement. The temperature distributions of SOFCs under different operating conditions (1023 K, 1073 K and 1123 K) are presented in Figure 6. It can be seen that the temperature increases firstly and then decreases along the x-coordinate direction for all three cases. This is attributed to the counter-flow arrangement of SOFCs. For the co-flow arrangement of SOFCs, the temperature gradually increases along the flow direction [5]. The maximum temperature occurs at the upstream of the fuel cell along the x-coordinate direction. And the maximum temperatures of three cases are 1080.1 K, 1189.9 K and 1334.8 K, respectively. It is also seen that the temperature gradient increases with increasing operating temperature.

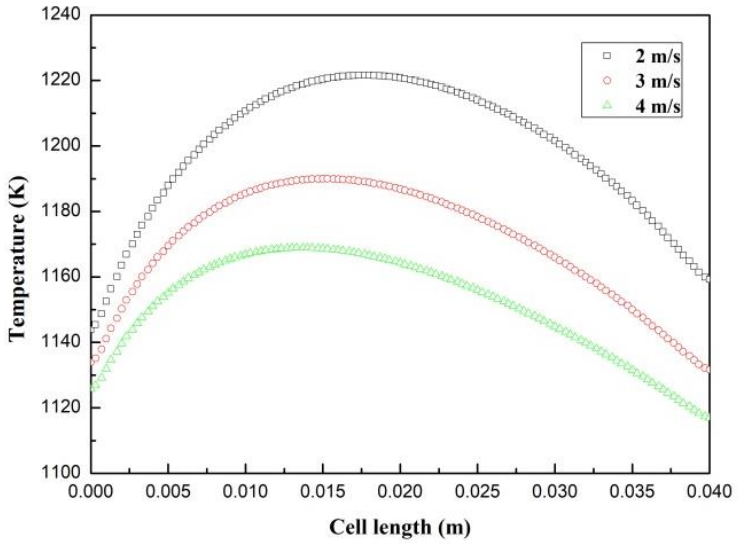

Figure 8. Temperature distributions at the anode DL and FL interface of SOFCs with different cathode inlet flow velocities at the cell voltage 0.7V.

The temperature distributions of SOFCs under different anode inlet flow velocities (0.2 m/s, 0.3 m/s and 0.4 m/s) are shown in Figure 7. In this study, the operating temperature is fixed at 1073 K for three cases. It is clearly seen that the local temperature decreases with increasing velocity, especially at the maximum temperature region. And the maximum temperatures of three cases are 1186.4 K, 1189.9 K and 1191.9 K, respectively. It is concluded that the local temperature can be decreased when the anode inlet flow velocity is increased. However, the effect of anode inlet flow velocity on temperature distribution can be neglected for the co-flow arrangement of SOFCs [5].

The temperature distributions of SOFCs under different cathode inlet flow velocities (2 m/s, 3 m/s and 4 m/s) are shown in Figure 8. In this study, the operating temperature is fixed at 1073 K for three cases. It is clearly seen that the local temperature greatly decreases with increasing velocity, especially at the maximum temperature region. And the maximum temperatures of three cases are 1221.5 K, 1189.9 K and 1168.8 K, respectively. It is also observed that the position of maximum temperature shifts towards the left with increasing velocity. It is concluded that the local temperature can be significantly decreased when the cathode inlet flow velocity is increased. Similarly, the local temperature is also decreased with increasing cathode inlet flow velocity for the co-flow arrangement of SOFCs [5]. Generally, different flow arrangements including co-flow, counter-flow and cross-flow can be used for SOFCs [23]. Therefore, it is also necessary to investigate the effects of operating temperature, anode inlet flow velocity and cathode inlet flow velocity on temperature distributions of SOFC with cross-flow arrangement.

4. CONCLUSIONS

In this study, the performance and transport characteristics of SOFCs with counter flow arrangement was numerically investigated. The results provided by the mathematical model show good agreement with the experimental data. The hydrogen and oxygen mass fractions decrease along the

corresponding gas flow directions, and the water vapor mass fraction increase along the anode channel due to the existence electrochemical reactions. The temperature gradient increases with increasing operating temperature. The local temperature decreases with increasing anode and cathode inlet flow velocities. It is also suggested that the cathode inlet flow velocity can be greatly increased to decrease the local temperature and then decrease the temperature gradient.

ACKNOWLEDGMENTS
The authors gratefully acknowledge the financial supports from National Natural Science Foundation of China (No.51606013 and No.51779025). This work is also funded by the Fundamental Research Funds for the Central Universities of China (No.3132019191, No.3132019187 and No. 3132019327), China Postdoctoral Science Foundation (No.2019M651097 and No.2019M651094) and Natural Science Foundation of Liaoning Province (No.2019-BS-026 and No.2019-ZD-0154).

References

1. O.Z. Sharaf, M.F. Orhan, *Renew. Sust. Energ. Rev.*, 32 (2014) 810.
2. Y. Wang, K.S. Chen, J. Mishler, S.C. Cho, X.C. Adroher, *Appl. Energy*, 88 (2011) 981.
3. S. Mekhilef, R. Saidur, A. Safari, *Renew. Sust. Energ. Rev.*, 16 (2012) 981.
4. Y.D. Hsieh, Y.H. Chan, S.S. Shy, *J. Power Sources*, 288 (2015) 1.
5. Q.W. Shen, S.A. Li, G.G. Yang, N.B. Huang, J.L. Yuan, B. Sunden, *Numer. Heat Transfer A*, 75 (2019) 509.
6. J.M. Park, D.Y. Kim, J.D. Baek, Y. Yoon, P. Su, and S. Lee, *Energies,* 11 (2018) 473.
7. Q.W. Shen, S.A. Li, G.G. Yang, N.B. Huang, *Int. J. Electrochem. Sci.*, 14 (2019) 5344.
8. W. Bi, D. Chen, Z. Jing, *Int. J. Hydrogen Energy*, 34 (2009) 3873.
9. C.M. An, J.H.Song, I. Kang, N. Sammes, *J. Power Sources*, 195 (2010) 821.
10. S. Lee, I. Park, H. Lee, D. Shin, *Int. J. Hydrogen Energy*, 39 (2014) 14342.
11. C. Wang, *Energies*, 9 (2016) 408.
12. J. Mccoppin, I. Barney, S. Mukhopadhyay, R. Miller, T. Reitz, D. Young, *J. Power Sources*, 215 (2012) 160.
13. J.R. Ferguson, J.M. Fiard, R. Herbin, *J. Power Sources*, 58 (1996) 109.
14. L. Andreassi, G. Rubeo, S. Ubertini, P. Lunghi, R. Bove, *Int. J. Hydrogen Energy*, 32 (2007) 4559.
15. I. Khazaee, and A. Rava, *Energy*, 119 (2017) 235.
16. Q.W. Shen, L.N. Sun, and B.W. Wang, *Int. J. Electrochem. Sci.*, 14 (2019) 1698.
17. H. Mahcene, H.B. Moussa, H. Bouguettaia, D. Bechki, S. Babay, M.S. Meftah, *Int. J. Hydrogen Energy*, 36 (2011) 4244.
18. S. Lee, H. Kim, K. J. Yoon, J. Son, J. Lee, B. Kim, W. Choi, J Hong, *Int. J. Heat Mass Transf.*, 97 (2016) 77.
19. Z. Zhang, J. Chen, D. Yue, G. Yang, S. Ye, C. He, W. Wang, J. Yuan, N. Huang, *Energies*, 7 (2014) 80.
20. S. Li, R. Wei, Y. Qi, G. Yang, Q. Shen, *Int. J. Electrochem. Sci.*, 14 (2019) 11367.
21. S. Li, J. Yuan, G. Xie, B. Sunden, *Int. J. Hydrogen Energy*, 43 (2018) 8451.
22. Z. Zhang, D. Yue, C. He, S. Ye, W. Wang, J. Yuan, *Heat Mass Transf.*, 50 (2014) 1575.
23. Z. Zhang, D. Yue, G. Yang, J. Chen, Y. Zheng, H. Miao, W. Wang, J. Yuan, N. Huang, *Int. J. Heat Mass Transf.*, 84 (2015) 942.